1-1-2017

Confined NaAlH4nanoparticles inside CeO2hollow nanotubes towards enhanced hydrogen storage

Qili Gao
Shanghai University

Guanglin Xia
University of Wollongong, guanglin@uow.edu.au

Xuebin Yu
Fudan University, xyu@uow.edu.au

Confined NaAlH4nanoparticles inside CeO2hollow nanotubes towards enhanced hydrogen storage

Abstract

NaAlH 4 has been widely regarded as a potential hydrogen storage material due to its favorable thermodynamics and high energy density. The high activation energy barrier and high dehydrogenation temperature, however, significantly hinder its practical application. In this paper, CeO 2 hollow nanotubes (HNTs) prepared by a simple electrospinning technique are adopted as functional scaffolds to support NaAlH 4 nanoparticles (NPs) towards advanced hydrogen storage performance. The nanoconfined NaAlH 4 inside CeO 2 HNTs, synthesized via the infiltration of molten NaAlH 4 into the CeO 2 HNTs under high hydrogen pressure, exhibited significantly improved dehydrogenation properties compared with both bulk and ball-milled CeO 2 HNTs-catalyzed NaAlH 4 . The onset dehydrogenation temperature of the NaAlH 4 @CeO 2 composite was reduced to below 100 °C, with only one main dehydrogenation peak appearing at 130 °C, which is 120 °C and 50 °C lower than for its bulk counterpart and for the ball-milled CeO 2 HNTs-catalyzed NaAlH 4 , respectively. Moreover, ∼5.09 wt% hydrogen could be released within 30 min at 180 °C, while only 1.6 wt% hydrogen was desorbed from the ball-milled NaAlH 4 under the same conditions. This significant improvement is mainly attributed to the synergistic effects contributed by the CeO 2 HNTs, which could act as not only a structural scaffold to fabricate and confine the NaAlH 4 NPs, but also as an effective catalyst to enhance the hydrogen storage performance of NaAlH 4 .

Disciplines

Engineering | Physical Sciences and Mathematics

Publication Details

Gao, Q., Xia, G. & Yu, X. (2017). Confined NaAlH4nanoparticles inside CeO2hollow nanotubes towards enhanced hydrogen storage. Nanoscale, 9 (38), 14612-14619.

Nanoscale

ARTICLE

Confined $NaAlH_4$ Nanoparticles inside CeO_2 Hollow Nanotubes towards Enhanced Hydrogen Storage

Received 00th January 20xx,
Accepted 00th January 20xx

DOI: 10.1039/x0xx00000x

www.rsc.org/

Qili Gao,[a] Guanglin Xia*[b] and Xuebin Yu*[a]

$NaAlH_4$ has been widely regarded as a potential hydrogen storage material due to its favorable thermodynamics and high energy density. The high activation energy barrier and high dehydrogenation temperature, however, significantly hinder its practical application. In this paper, CeO_2 hollow nanotubes (HNTs) prepared by a simple electrospinning technique are adopted as functional scaffolds to support $NaAlH_4$ nanoparticles (NPs) towards advanced hydrogen storage performance. The nanoconfined $NaAlH_4$ inside CeO_2 HNTs, synthesized via the infiltration of molten $NaAlH_4$ into the CeO_2 HNTs under high hydrogen pressure, exhibited significantly improved dehydrogenation properties compared with both bulk and ball-milled CeO_2 HNTs-catalyzed $NaAlH_4$. The onset dehydrogenation temperature of the $NaAlH_4$@CeO_2 composite was reduced to below 100 °C, with only one main dehydrogenation peak appearing at 130 °C, which is 120 °C and 50 °C lower than for its bulk counterpart and for the ball-milled CeO_2 HNTs-catalyzed $NaAlH_4$, respectively. Moreover, ~ 5.09 wt.% hydrogen could be released within 30 min at 180 °C, while only 1.6 wt.% hydrogen was desorbed from the ball-milled $NaAlH_4$ under the same conditions. This significant improvement is mainly attributed to the synergistic effects contributed by the CeO_2 HNTs, which could act as not only a structural scaffold to fabricate and confine the $NaAlH_4$ NPs, but also as an effective catalyst to enhance the hydrogen storage performance of $NaAlH_4$.

Introduction

Considering the increasing energy demands of human societies, it is an urgent necessity to find an alternative to the limited sources of fossil fuels. Hydrogen has been widely recognized as one of the most promising renewable, environmentally friendly energy carriers, owing to its high energy content.[1-5] In order to realize the widespread utilization of hydrogen, one of the main challenges has been how to store hydrogen safely and efficiently. In comparison with cryogenically liquefied hydrogen or highly compressed hydrogen technologies, hydrogen storage in solid-state materials is attracting an increasing amount of attention due to its high energy density and unique safety characteristics.

Sodium alanate ($NaAlH_4$), which possesses high gravimetric (ρ_m = 7.5 wt.% H_2) and volumetric (ρ_v = 94 gH_2 L^{-1}) hydrogen densities with moderate thermodynamic properties, is regarded as one of the most promising solid-state hydrogen-storage materials. The equilibrium chemical reactions of $NaAlH_4$ for hydrogen storage are shown in the following equations:

$$NaAlH_4 \leftrightarrow 1/3\ Na_3AlH_6 + 2/3\ Al + H_2\ (3.7\ wt.\%) \quad (1)$$

$$Na_3AlH_6 \leftrightarrow 3\ NaH + Al + 3/2\ H_2\ (1.9\ wt.\%) \quad (2)$$

$$NaH \rightarrow Na + 1/2\ H_2\ (1.9\ wt.\%) \quad (3)$$

Because the decomposition temperature of NaH exceeds 300 °C, only the first two reversible reaction steps are suitable for practical applications. Accordingly, the hydrogen storage capacity of $NaAlH_4$ for practical application approaches approximately 5.6 wt.%.[6,7] The slow dehydrogenation/ hydrogenation kinetics and poor reversibility, however, significantly impede the application of $NaAlH_4$ as a hydrogen storage material.

The pioneering work of Bogdanović and Schwickardi has demonstrated that Ti-doped $NaAlH_4$ is capable of reversible hydrogen storage under mild conditions.[6] Subsequently, a series of catalysts was employed to further improve the hydrogen storage properties of $NaAlH_4$. Recently, it has been verified that Ce-based catalysts are superior to $TiCl_3$ in terms of enhancing the hydrogen storage performance of $NaAlH_4$.[11] For example, the introduction of CeO_2 nanoparticles (NPs) could lower the dehydrogenation temperature of $NaAlH_4$ down to around 100 °C and induce further enhancement of its hydriding and dehydriding kinetics.[12] Furthermore, Zhang et al. prepared a nanocrystalline CeO_2@C-containing $NaAlH_4$ composite, by hydrogenating a NaH-Al mixture doped with CeO_2@C.[13] This composite could rapidly release approximately ~ 4.7 wt.% hydrogen at temperatures ranging from 95 to 190 °C under dynamic heating, and the onset dehydrogenation temperature could be reduced to only 77 °C.

In addition to the adoption of catalytic agents, nanoconfinement has been proved to be an effective

[a] Department of Materials Science, Fudan University, Shanghai 200433 , China. E-mail: yuxuebin@fudan.edu.cn
[b] Institute for Superconducting and Electronic Materials, University of Wollongong, North Wollongong, NSW 2522, Australia. E-mail: guanglin@uow.edu.au

† Electronic Supplementary Information (ESI) available. See DOI: 10.1039/x0xx00000x

approach to improving both the kinetics and thermodynamics of the hydrogen storage reactions of $NaAlH_4$.[10,29,35] This strategy is mainly achieved via wet impregnation or melt infiltration of $NaAlH_4$ into various kind of scaffold materials, which could significantly decrease the particle size of $NaAlH_4$ by taking advantage of the structural support of scaffolds. As early as 2006, Baldé et al. investigated the hydrogen absorption and desorption characteristics of $NaAlH_4$ supported by surface-oxide carbon nanofibers, which exhibited a hydrogen storage capacity of 3.7 wt.% of hydrogen below 160 °C.[14] Subsequently, various carbon nanomaterials, such as carbon nanofibers,[16] porous carbon,[19,23] carbon aerogels,[24-25] and C_{60},[20] as well as metal organic frameworks (MOF), such as MOF-74 (Mg)[27] and $Cu_3(BTC)_2$ MOF,[28] and ordered mesoporous silica, were used to support and confine $NaAlH_4$ to enhance both the kinetics and the thermodynamics of dehydrogenation.[15] The reduction of particle size down to the nanoscale, induced by nanoconfinement, could significantly decrease the hydrogen diffusion distance, leading to tremendously improved kinetics for hydrogenation and dehydrogenation. Remarkably, it has been demonstrated that the addition of catalysts, i.e., $TiCl_3$, into porous scaffolds could further improve the hydrogen storage performance of nanoconfined $NaAlH_4$, decreasing the peak temperature for dehydrogenation to 125 °C, which is 34 °C lower than for nanoconfined $NaAlH_4$ without $TiCl_3$.[29] This result indicates that the combination of catalysts and nanoconfinement could have a synergetic effect towards improving the hydrogenation and dehydrogenation performance of $NaAlH_4$. Nonetheless, it should be pointed out that the inhomogeneous distribution of catalysts in these scaffolds leads to a limited catalytic effect on the nanoconfined $NaAlH_4$. Therefore, it is highly desirable to develop catalytic structural supports to confine $NaAlH_4$, which could result in intimate contact between $NaAlH_4$ nanoparticles on the inside and the catalyst, leading to advanced hydrogen storage performance.

In this work, porous CeO_2 hollow nanotubes (HNTs), as catalytic nanoscaffolds, were fabricated to improve the hydrogen storage performance of $NaAlH_4$. Taking advantage of the porous nanostructure and thermal stability of CeO_2 HNTs, the molten $NaAlH_4$ can be homogeneously filled into the CeO_2 HNTs by thermal melt impregnation under high-pressure H_2, with the product denoted as $NaAlH_4$@CeO_2. Induced by the reduction of the particle size of $NaAlH_4$ to nanometer range as well as the catalytic effects of CeO_2, the $NaAlH_4$@CeO_2 could release approximately 5.09 wt.% hydrogen within 30 min at 180 °C, with the dehydrogenation onset temperature decreased to about 75 °C, which is 55 °C and 95 °C lower than for bulk $NaAlH_4$ and ball-milled $NaAlH_4$/CeO_2, respectively.

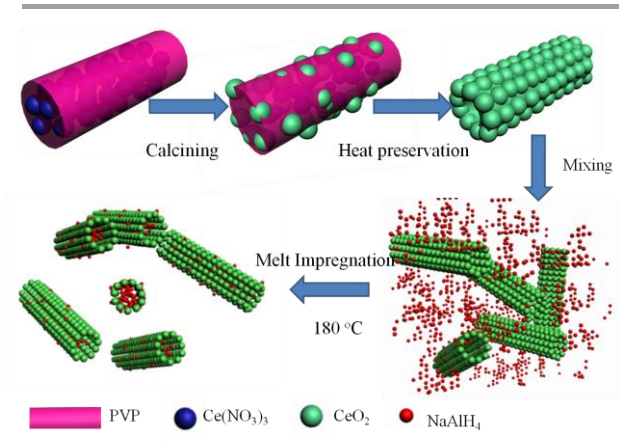

Fig. 1 Schematic illustration of the synthesis process for $NaAlH_4$@CeO_2.

Experimental section

Preparation of CeO_2 HNTs

In order to synthesize CeO_2 HNTs, a two-step process was adopted, which included a simple one-step electrospinning process and an annealing process. In the first step, 1 mmol of cerium nitrate hexahydrate ($Ce(NO_3)_3$ $6H_2O$, Sigma-Aldrich Inc., USA) was dissolved in 10 mL of N,N-dimethylformamide (DMF) with magnetic stirring at room temperature for 30 min. Then, an appropriate amount of polyvinylpyrrolidone (PVP, Mw ≈ 1300000, Sigma-Aldrich Inc., USA) was added into the mixed solution. The weight ratio of PVP to inorganic salt was 3. Finally, a homogenous precursor solution was obtained after vigorous magnetic stirring for 3 h. The viscous composite solution was poured into a syringe equipped with an 18-gauge blunt-tip stainless steel needle. The flow rate of solution was approximately 500 $\mu L h^{-1}$, controlled by a syringe pump (Longer, TJP-3A, China). During the electrospinning process, the needle and a collector plate were connected to a high-voltage generator. In this case, a voltage of 16 kV was applied between the cathode (metal collector plate) and the anode (needle) with a collection distance of 15 cm. The precursor solution was ejected from the needle under the effect of the high voltage that was applied. With the evaporation of solvent, the solution jet solidified on the collector. The whole experiment was conducted in an extremely dry environment. After the collected samples were dried for 12 h at 80 °C under vacuum, the fibers were annealed in a tube furnace with a temperature ramp rate of 1 °C min^{-1} from room temperature to 600 °C and sintered for 3 h. The slow heating rate could ensure that the organic phase was removed, without destroying the structure of the nanofibers. After cooling down to room temperature, the nanotubes were formed.

Nanoconfinement of $NaAlH_4$ in CeO_2 HNTs

$NaAlH_4$ was confined in short CeO_2 HNTs by the following thermal melt-impregnation process. Typically, a mixture of $NaAlH_4$ (95 % purity, Sigma–Aldrich) and as-prepared CeO_2 HNTs, with a mass ratio of 1:1, was obtained by manual grinding. Then, the mixture was loaded into and sealed in a stainless-steel autoclave in an N_2-filled glove box. The stainless-steel autoclave was subsequently evacuated and refilled with H_2 (99.999 % purity) to 3.5 MPa to prevent the

decomposition of $NaAlH_4$ during the heating process. After that, the autoclave was heated to 180 °C (close to the melting temperature of $NaAlH_4$) from room temperature with a heating rate of 5 °C min^{-1} and kept at this temperature for 30 min. This operation was repeated three times, which could impregnate the molten $NaAlH_4$ into the CeO_2 HNTs as a result of capillary action. After cooling to room temperature, the autoclave was transferred back into the glove box, where the infiltrated sample, denoted as $NaAlH_4$@CeO_2, could be collected.

Preparation of the ball-milled sample

The CeO_2 HNTs and $NaAlH_4$ with a mass ratio of 1:1 were introduced into a stainless steel vessel together with stainless steel balls in an N_2-filled glove box. The milling was carried out at 350 rpm, and the ball-to-powder weight ratio was 50:1. After 12 h of milling, the sample was obtained and denoted as $NaAlH_4$/CeO_2.

Characterizations

The composition of powdered samples was investigated on an X-ray diffractometer (XRD; D8 Advance, Bruker AXS) with Cu Kα radiation at 50 kV and 30 mA. The preparation of samples for XRD measurements was entirely conducted in an N_2-filled glove box, and the surfaces of samples were covered with Scotch tape to protect the samples from moisture and air. Fourier transform infrared (FTIR) spectra were collected at room temperature by using a FTIR-650 spectrometer (Tianjin Gangdong) at a resolution of 4 cm^{-1}. The morphology, microstructure, and elemental distribution were analysed on a JEOL JEM-2100F transmission electron microscope (TEM) and a Shimadzu JEOL 7500FA scanning electron microscope (SEM). For the TEM measurements, the samples were dispersed in dried acetone solvent by ultrasonic treatment, and then spread on a copper grid. For SEM measurements, the samples were dispersed on electrically conducting adhesive tape. All the samples in the glove box were rapidly transferred into the equipment, which was filled with N_2, and then they were diverted into the chambers for TEM and SEM measurements as soon as possible. The distribution of elemental O, Ce, Na, and Al in the samples was detected with an energy-dispersive X-ray spectrometer (EDS) attached to the TEM. Mass spectrometer analysis (MS; Hiden HPR 20), in conjunction with thermogravimetric analysis (TG; Netzsch STA449 F3), was protected by N_2 gas, flowing at the rate of 80 mL min^{-1}, with a heating rate of 5 °C min^{-1}. The kinetic properties were measured by a volumetric method based on Sieverts' law using an automatic device from SUZUKI HOKAN.CO., LTD. in Japan. The H_2 desorption kinetics properties were measured at various temperatures with an H_2 pressure around 0.01 atm. For comparison, the weight of CeO_2 was excluded in the calculation of dehydrogenation capacity from the $NaAlH_4$@CeO_2 and $NaAlH_4$/CeO_2.

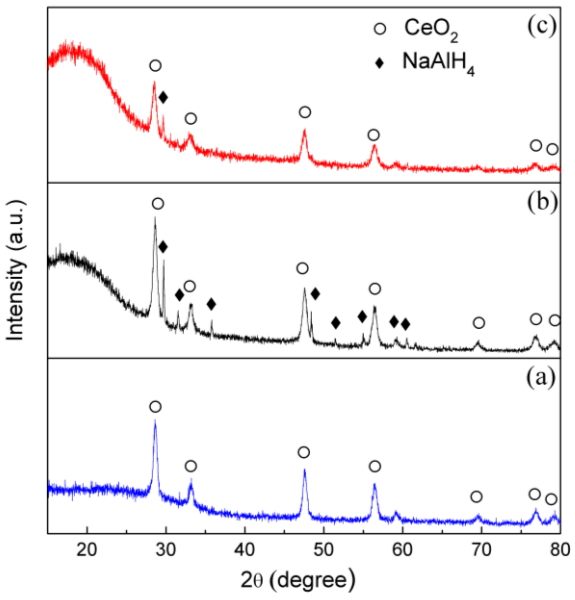

Fig. 2 XRD patterns for the samples: (a) as-prepared CeO_2, (b) ball-milled $NaAlH_4$/CeO_2, and (c) as-prepared $NaAlH_4$@CeO_2.

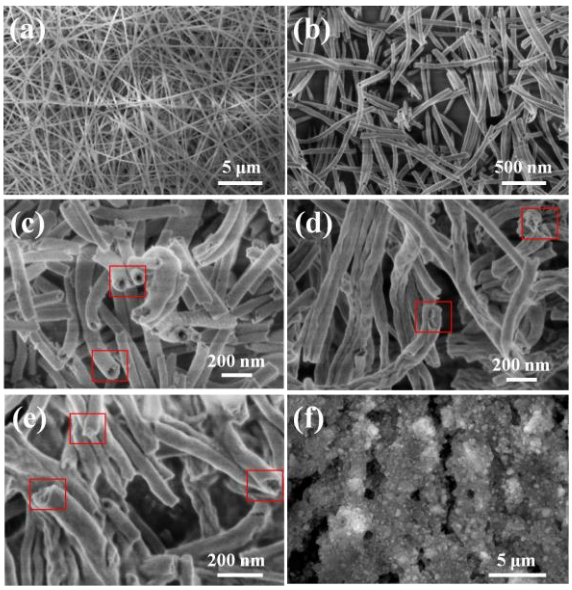

Fig. 3 SEM images of the precursor PVA-$Ce(NO_3)_3$ nanofibers (a), as-prepared CeO_2 (b, c), as-prepared $NaAlH_4$@CeO_2 (d, e), and as-milled $NaAlH_4$/CeO_2 (f). The characteristics of the cross-sections of CeO_2 fibers are marked with red boxes.

Results and discussion

Synthesis and characterization of $NaAlH_4$@CeO_2

As shown in Fig. 1, CeO_2 HNTs were synthesized by annealing the precursor, i.e., PVA-$Ce(NO_3)_3$ nanofibers, via tuning the heating rate and annealing temperature. Firstly, PVA-$Ce(NO_3)_3$ nanofibers were heated to 600 °C at a rate of 1 °C min^{-1} to remove the PVP. During this process, the rate of decomposition of PVP was higher than the gas diffusion through the fiber surface, owing to the slow heating rate, and therefore, the pressure inside the nanofibers increased faster than that outside of the composite fibers, leading to the constriction of outside nanoparticles.[32-34] Subsequently, the

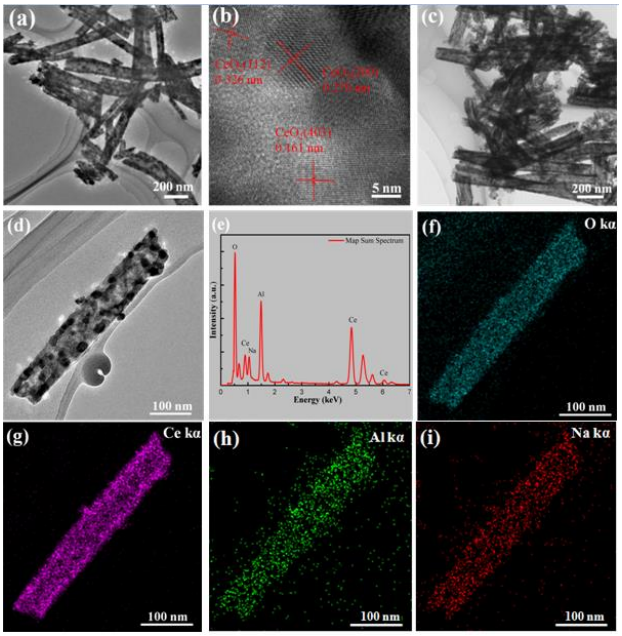

Fig. 4 TEM images of CeO_2 (a) and $NaAlH_4$@CeO_2 (c, d), HRTEM image of CeO_2 (b), EDS spectrum (e), and the corresponding EDS maps of (f) O, (g) Ce, (h) Al, and (i) Na elements for image (d).

precursor was calcined at 600 °C for 3 h to synthesize nanocrystalline CeO_2. Due to the rapid increase in the reaction rate at 600 °C, the particles inside expanded owing to the large strain and Ostwald ripening, leading to the formation of nanotubes.[33-34] The X-ray diffraction (XRD) pattern of the as-prepared CeO_2 HNTs, as shown in Fig. 2a, exhibits the characteristic diffraction peaks of CeO_2 (PDF 34-0394), which confirms the formation of CeO_2 crystallites. The SEM (Fig. 3a-c) images reveal that both the as-synthesized PVA-$Ce(NO_3)_3$ nanofibers and the CeO_2 HNTs exhibit uniform fibrous structures, with a diameters of ~ 300 nm and 70 nm, respectively. The hollow structure of the as-synthesized CeO_2 nanofibers could be verified from the cross-sections of some broken fibers (Fig. 3b-c). The TEM image further demonstrates the formation of CeO_2 HNTs (Fig. 4a), which confirms that the thickness of the walls of the as-synthesized CeO_2 HNTs, composed of CeO_2 NPs with a diameter of ~ 13 nm, is approximately 17 nm. By analyzing the high-resolution TEM (HRTEM) images (Fig. 4b), the interplanar spacings of the nanoparticles were measured to be 0.326 nm, 0.270 nm, and 0.161 nm, corresponding to the (112), (200), and (403) planes of CeO_2, respectively, which provides further evidence for the formation of CeO_2 nanocrystals. According to the above observations, it is concluded that the CeO_2 HNTs were synthesized successfully.

The XRD pattern in Figure 2b shows that the as-prepared $NaAlH_4$/CeO_2 composite presents the typical peaks belonging to CeO_2 and $NaAlH_4$. Because the particle size of $NaAlH_4$ remains large, the diffraction peaks are obvious and sharp, which is similar to the pure $NaAlH_4$. In comparison, although the characteristic peaks of CeO_2 are still observed, only weak and broad peaks indexed to $NaAlH_4$ are present in the $NaAlH_4$@CeO_2 (Fig. 2c). This indicates the loss of the crystalline structure of $NaAlH_4$ due to the melt infiltration process and the significant reduction in the particle size down to nanometer range that was induced by nanoconfinement by the CeO_2 HNTs.[22-23]

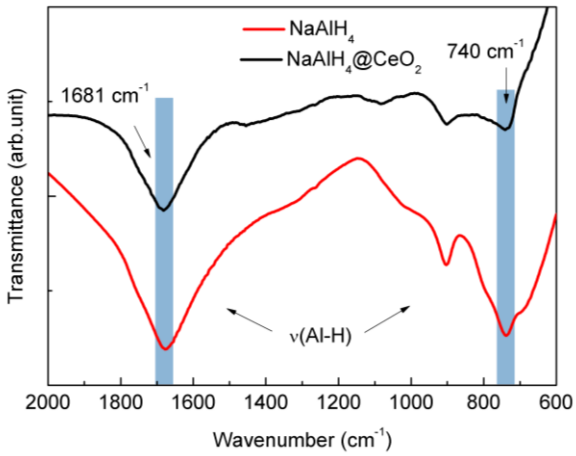

Fig. 5 FTIR spectra of the bulk $NaAlH_4$ and as-prepared $NaAlH_4$@CeO_2.

Therefore, Fourier transform infrared spectroscopy (FTIR) was further adopted to characterize the presence of $NaAlH_4$ inside the CeO_2 HNTs in $NaAlH_4$@CeO_2. Fig. 5 displays the FTIR spectra of the bulk $NaAlH_4$ and the as-prepared $NaAlH_4$@CeO_2 in the wavenumber range of 600–2000 cm^{-1}. The peaks of the bulk $NaAlH_4$ at 1676 cm^{-1} and 738 cm^{-1} correspond to the stretching mode ν_3 of the Al–H vibration and the bending mode ν_4 of the AlH_4 group, respectively. After melt infiltration of $NaAlH_4$ into the CeO_2 HNTs, these two peaks could be clearly observed, but slightly shifted to higher wavenumbers, which indicates the presence of $NaAlH_4$ phase in the CeO_2 HNTs after the infiltration process without decomposition. Furthermore, as shown in Fig. S3, after infiltration of $NaALH_4$, BET specific surface area and BJH total pore volume decreased from 24 to 2.5 m^2 g^{-1} and 0.063 cm^3 g^{-1} to 0.0079 cm^3 g^{-1}, respectively, which indicates the confinement of $NaAlH_4$ into the CeO_2 tubes.

The morphology and structure of the nanoconfined $NaAlH_4$ NPs inside the CeO_2 HNTs were further investigated by SEM (Fig. 3d-e) and TEM (Fig. 4). It could be clearly observed from the cross-section of the as-prepared $NaAlH_4$@CeO_2 (Fig. 3d-e) that $NaAlH_4$ NPs had successfully filled the hollow cavities and the wall defects of the CeO_2 HNTs without any aggregation, with a fraction of the $NaAlH_4$ NPs deposited on the external surfaces of these nanotubes. EDS analysis (Fig. 4e) demonstrates the presence of the elements Ce, O, Al, and Na inside the CeO_2 HNTs, suggesting the encapsulation of $NaAlH_4$ in the CeO_2 HNTs in $NaAlH_4$@CeO_2. The scanning TEM (STEM) image (Fig. 4d), combined with the corresponding EDS mapping results for the O, Ce, Na, and Al elements of the $NaAlH_4$@CeO_2 sample, as shown in Fig. 4f-i, confirms that all four element maps apparently match very well with the shape of the as-prepared $NaAlH_4$@CeO_2, indicating the homogeneous distribution of $NaAlH_4$ inside the CeO_2 HNTs. Specifically, both the Na-map and the Al-map, originating

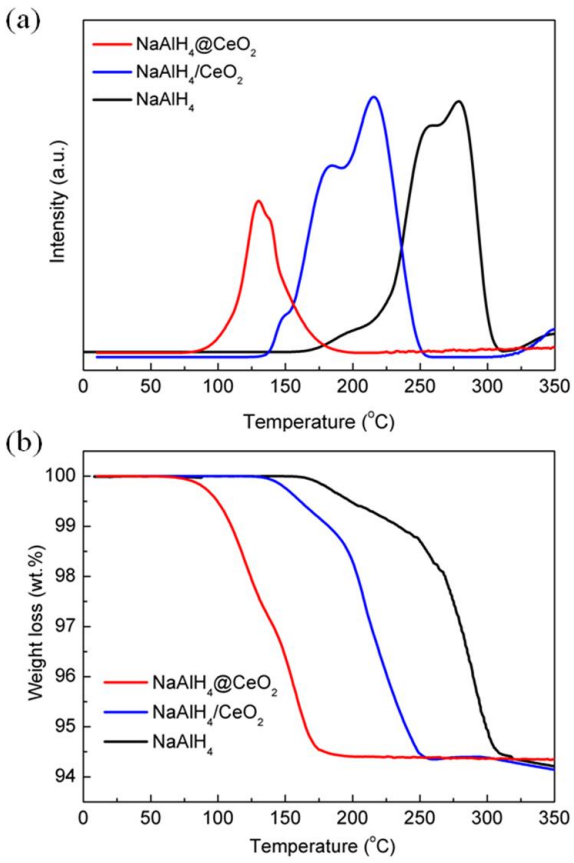

Fig. 6 MS curves (a) and TG curves (b) for bulk $NaAlH_4$, $NaAlH_4/CeO_2$, and $NaAlH_4@CeO_2$, with a heating rate of 5 °C min^{-1}.

from the $NaAlH_4$ NPs, are slightly different from the O-map and Ce-map originating from the CeO_2 HNTs, in which the element densities at the edges of the nanotubes are larger than in the middle of the tubes. This difference indicates that a large percentage of the $NaAlH_4$ NPs were embedded and well dispersed inside the interior cavities of the nanotubes, with only a small part of the Na and Al distributed on the outside of the CeO_2 HNTs, which coincides well with the SEM results.

In order to investigate the hydrogen storage properties of the as-prepared $NaAlH_4@CeO_2$, both mass spectroscopy (MS) and thermogravimetric analysis (TGA) (Fig. 6) were conducted with the bulk $NaAlH_4$ and the milled $NaAlH_4/CeO_2$ composite included for comparison. As expected, the decomposition of bulk $NaAlH_4$ started at around 170 °C, and two dehydrogenation peaks at about 250 °C and 280 °C (Fig. 6a), corresponding to the stepwise reactions shown in Eqs. (1-2), respectively, were observed, which agrees well with the reported values.[22] Compared with the bulk $NaAlH_4$, the ball-milled $NaAlH_4/CeO_2$ composite showed significantly improved dehydrogenation behaviour, with the onset dehydrogenation temperature reduced to 130 °C, which was 40 °C lower than for its bulk counterpart. Moreover, the peak temperatures for the initial two dehydrogenation reactions were decreased to 180 °C and 213 °C, which are 70 °C and 67 °C lower than for the bulk $NaAlH_4$, respectively. This result obviously verifies the catalytic effect of CeO_2 on the dehydrogenation of $NaAlH_4$, in good agreement with the previous reports.[12, 13, 40] In strong contrast, the MS result indicates that the process of hydrogen desorption of $NaAlH_4@CeO_2$ took place at a much lower temperature of approximately 75 °C, and only one distinct main peak was observed at about 130 °C, which were both significantly lower than for the milled $NaAlH_4/CeO_2$ composite. Additionally, it is remarkable that the first two decomposition steps of $NaAlH_4$ tended merged into one single hydrogen release step for the as-prepared $NaAlH_4@CeO_2$, comparing with $NaAlH_4@CeO_2$ and bulk $NaAlH_4$.[19,26,31] It has been calculated that when particle size was reduced to less than 50 nm, $NaAlH_4$ could decompose in a single step to directly form NaH and Al at a temperature below its melting point (~ 180 °C) in reported papers.[34] Due to Jahn-Teller distortion in small clusters, the decomposition of $NaAlH_4$ may occur in a single step, without any Na_3AlH_6 intermediate.[30] Therefore, these results directly demonstrate the synergetic effects of the catalysis and nanoconfinement provided by CeO_2 HNTs towards significantly enhancing the dehydrogenation properties of $NaAlH_4$.

The TGA curves (Fig. 6b) demonstrate that the first two stages of hydrogen release were completed at around 310 °C

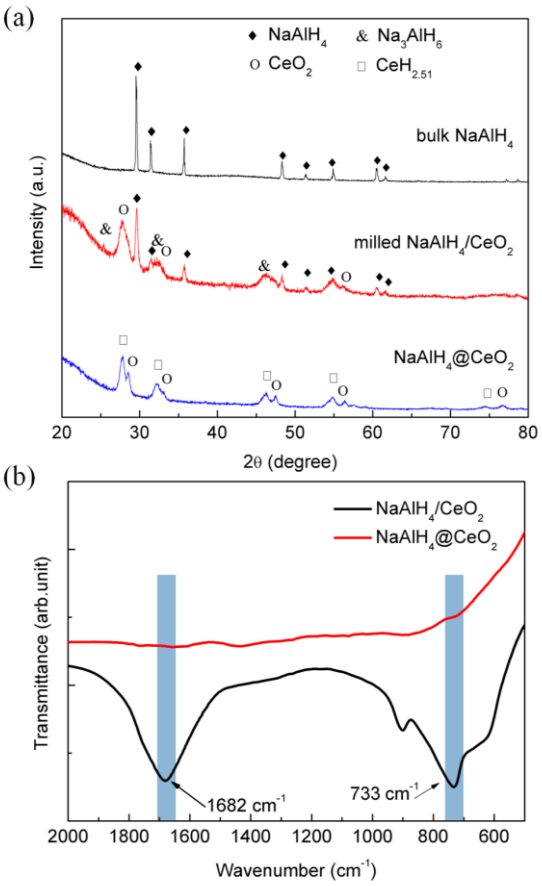

Fig. 7 (a) XRD patterns of the dehydrogenated products of bulk $NaAlH_4$, the ball-milled $NaAlH_4/CeO_2$ composite, and $NaAlH_4@CeO_2$at 200 °C; (b) FTIR spectra of the dehydrogenated products of the ball-milled $NaAlH_4/CeO_2$ and $NaAlH_4@CeO_2$ at 200 °C.

for the bulk $NaAlH_4$, and a total amount of approximately 5.6 wt.% H_2 is evolved, which coincides well with its theoretical capacity. It should be noted that all the hydrogen capacity is calculated based on the $NaAlH_4$ in the composite. By comparison, 5.5 wt.% hydrogen could be released from $NaAlH_4/CeO_2$ composite at temperatures below 250 °C. In addition, the onset temperature declined from 175 °C for the bulk $NaAlH_4$ to 130 °C for the $NaAlH_4/CeO_2$ composite, suggesting that the presence of CeO_2 provided effective catalytic effects towards the decomposition of the $NaAlH_4$ and Na_3AlH_6. In terms of $NaAlH_4@CeO_2$, the desorption kinetics were significantly enhanced, which is supported by the decrease of the onset dehydrogenation temperature to below 80 °C and the completion of the dehydrogenation process at a temperature as low as 180 °C. The hydrogen capacity released based on the $NaAlH_4$ in $NaAlH_4@CeO_2$ approaches ~ 5.45 wt.%, indicating complete dehydrogenation. These features correspond well with the MS results, demonstrating the tremendously improved dehydrogenation performance of $NaAlH_4$ owing to the homogeneous nanoconfinement of $NaAlH_4$ in CeO_2 HNTs.

In order to elucidate the mechanism by which the nanoconfinement of $NaAlH_4$ in CeO_2 HNTs enhances the dehydrogenation properties, the XRD patterns of bulk $NaAlH_4$, the ball-milled $NaAlH_4/CeO_2$ composite, and the as-prepared $NaAlH_4@CeO_2$, collected at 200 °C, are shown in Fig. 7a. Only $NaAlH_4$ is present for bulk $NaAlH_4$ upon heating to 200 °C, indicating that no dehydrogenation occurred at this temperature. The complete dehydrogenation of bulk $NaAlH_4$ could be achieved upon heating to 350 °C (Fig. S1 in the Supporting Information) as verified by the formation of NaH (JCPDS 02-0809) and Al (JCPDS 65-2869) without the presence of $NaAlH_4$, which agrees well with the TG and MS results. For the ball-milled $NaAlH_4/CeO_2$ composite, characteristic reflections of Na_3AlH_6 and $NaAlH_4$ are observed, suggesting the partial decomposition of $NaAlH_4$ under the catalytic effects of CeO_2. In the case of the as-prepared $NaAlH_4@CeO_2$, only peaks of CeO_2 and $CeH_{2.51}$ (JCPDS 32-0190) phases appeared, with the absence of any peaks for $NaAlH_4$ and/or Na_3AlH_6 after heating to 200 °C. It could be clearly observed that after dehydrogenation at 100 °C (Fig. S4), which is approaching the onset dehydrogenation temperatures, weak $CeH_{2.51}$ peaks for the sample after dehydrogenation at 100 °C were observed, attributed to the reaction between NaH and CeO_2.[12-13,40] It indirectly indicates the generation of NaH at only 100 °C. Comparing with previous report,[11] in which the Na_3AlH_6 and NaH are formed at 136 °C and 150 °C, respectively, the NaH is formed at a much lower temperature in the as-prepared $NaAlH_4@CeO_2$, and Na_3AlH_6 phase can be hardly detected, which is in accordance with the theoretical calculation prediction.[38] The destabilization of Na_3AlH_6 and NaH leads to a fast decomposition of $NaAlH_4$. Based on the FTIR results (Fig. 7b), all the peaks belonging to Al–H bonds of $NaAlH_4@CeO_2$ disappeared after dehydrogenation at 200 °C, which suggests the complete decomposition of the $NaAlH_4$. By comparison, the peaks of the Al–H bonds of $NaAlH_4/CeO_2$ at 1682 cm^{-1} and 733 cm^{-1} are still present upon heating to 200 °C in the FTIR spectra, which corresponds well to the XRD results. Notably, no well crystallized Al phase was observed in the dehydrogenated products of $NaAlH_4@CeO_2$, which indirectly confirms that the Al grains did not agglomerate into large particles due to the nanoconfinement by CeO_2 HNTs, providing structural support for the uniform distribution of $NaAlH_4$. Furthermore, as shown in Fig. S2, the hollow nanotube structure of CeO_2 was still well preserved after the dehydrogenation process. This indicates the high thermal stability induced by the physical contact between the $NaAlH_4$ and the CeO_2 HNTs. Besides, the homogeneous distribution of O, Ce, Al and Na in the original and dehydrogenated $NaAlH_4@CeO_2$ indicates that CeO_2 HNTs prevent the phase segregation of $NaAlH_4$. CeO_2 HNTs could serve as "nano-reactor"[23], where $NaAlH_4$ particles are limited to a nanoscale level which facilitates the interaction between $NaAlH_4$ and CeO_2 and shortens the H_2 diffusion distance, to achieve the sample with excellent kinetics. What's more, it should be noted that the presence of $CeH_{2.51}$ phase on the external surfaces to some extent could act as active species in the following hydrogen storage process.[13,36,37]

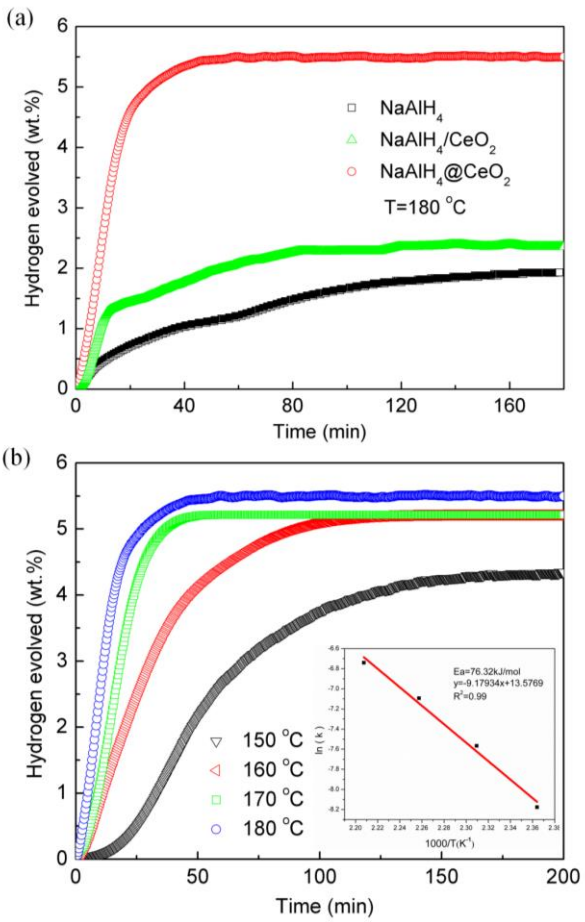

Fig. 8 Hydrogen desorption (under 0.01 atm hydrogen pressure) curves of the bulk $NaAlH_4$, ball-milled $NaAlH_4/CeO_2$, and $NaAlH_4@CeO_2$ at 180 °C (a). Hydrogen desorption kinetic curves of the $NaAlH_4@CeO_2$ at different temperatures (b). The inset shows the Arrhenius plot according to the isothermal H_2 desorption of $NaAlH_4@CeO_2$.

Isothermal dehydrogenation kinetics of $NaAlH_4$@CeO_2

The isothermal dehydrogenation properties (Fig. 8a) of the $NaAlH_4$@CeO_2, in comparison to the bulk $NaAlH_4$ and the milled $NaAlH_4$/CeO_2, were further investigated using a Sieverts' pressure-composition-temperature (PCT) apparatus at various temperatures. Specifically, the ball-milled $NaAlH_4$/CeO_2 composite released about 1.22 wt.% H_2 in less than 10 min, while there was no distinct signs of hydrogen release for the bulk $NaAlH_4$ within the initial 10 min at 180 ^{o}C. This further demonstrates the catalytic effects of CeO_2 towards the dehydrogention of $NaAlH_4$. The hydrogen desorption rate of $NaAlH_4$/CeO_2 fell drastically after 10 min, and only a small amount of hydrogen was slowly released in the following 100 min, according to Eq. (2), whereas the dehydrogenation of $NaAlH_4$@CeO_2 carried on at a higher rate throughout the whole process and was completed within 50 min. The amount of hydrogen released from the milled $NaAlH_4$/CeO_2 was 1.6 wt.% in 30 min, while the hydrogen capacity of the $NaAlH_4$@CeO_2 reached 5.09 wt.% through the same operation time at 180 ^{o}C, which was nearly three times as much as in the former case. In addition, only one hydrogen desorption step was observed in the dehydrogenation curve of $NaAlH_4$@CeO_2, which is in agreement with the MS results. These results directly demonstrate that the nanoconfinement effect of the CeO_2 HNTs is significantly effective towards enhancing the hydrogen storage performance of $NaAlH_4$.

The dehydrogenation outlines of the $NaAlH_4$@CeO_2 at 150, 160, 170, and 180 ^{o}C are presented in Fig. 8b. ~ 0.7 wt.% hydrogen was released from $NaAlH_4$@CeO_2 at 150 ^{o}C in 30 min, while the outcome went up to ~ 2.9 wt.% and ~ 4.6 wt.% at 160 and 170 ^{o}C, respectively, which is much better than for the reported dehydrogenation properties of $NaAlH_4$ using other scaffold materials for the mesoporous matrix.[23] Finally, 2.16 wt.%, 5.21 wt.%, and 5.22 wt.% of hydrogen could be desorbed at 150, 160, and 170 ^{o}C, respectively. When the temperature was increased to 180 ^{o}C, 5.09 wt.% hydrogen could be rapidly released within 30 min, and the whole hydrogen capacity of 5.51 wt.% could be achieved, approaching the theoretical value of 5.6 wt.%, in good agreement with the MS and TG results (Fig. 6). The apparent activation energy (E_a) for the hydrogen release reaction is calculated by configuring the isothermal dehydriding curves at different temperatures for the quantitative evaluation of the considerably improved dehydriding kinetics of the as-prepared $NaAlH_4$@CeO_2, using the Johanson–Mehl–Avrami-Kolmogorov (JMAK) Equation (4):

$$\alpha(t) = 1 - \exp[-(kt)^n] \quad (4)$$

Eq. (4) can be reformulated as:

$$\ln[-\ln(1-\alpha(t))] = n \ln t + n \ln k \quad (5)$$

where α is the reacted fraction with respect to time t, k is the rate constant, and n is the *Avrami* exponent, which is commonly used to discern the dehydrogenation mechanism. On plotting $\ln[-\ln(1-\alpha(t))]$ against $\ln t$, good linearity was achieved over the range of $0.03 \le \alpha \le 0.8$, with a correlation coefficient of $R^2 > 0.99$. Subsequently, the apparent activation energy was calculated to be approximately 76.32 kJ·mol^{-1} for the $NaAlH_4$@CeO_2, based on the slopes ($-E_a/R$), where R is the gas constant, of the straight lines according to *Arrhenius* equation (inset of Fig. 8b), which is much lower than the values reported for CeO_2@C doped-$NaAlH_4$ (E_{a1} = 90.3 kJ·mol^{-1} and E_{a2} = 81.7 kJ·mol^{-1}) obtained by ball milling[11] and bulk $NaAlH_4$[20]. The significant decrease in the apparent E_a directly verifies the improvement of the dehydrogenation kinetics due to the synergistic effects of nanoconfinement and the catalytic effects of CeO_2 HNTs.

Conclusions

In summary, this work investigates the adoption of CeO_2 HNTs as effective catalytic nanoscaffolds to improve the hydrogen storage performance of $NaAlH_4$. The hollow nanotube structure of the CeO_2 HNTs could act not only as a structural support to synthesize and stabilize the $NaAlH_4$ nanoparticles, but also as an effective catalyst to further enhance the hydrogen storage properties of nanosized $NaAlH_4$. Owing to the synergistic effects contributed by the CeO_2 HNTs towards improving the dehydrogenation properties of $NaAlH_4$, the hydrogen storage performance of $NaAlH_4$ is significantly improved. For instance, the onset temperature of dehydrogenation for the $NaAlH_4$@CeO_2 was reduced to 75 ^{o}C, which is ~ 95 ^{o}C and ~ 55 ^{o}C lower than for bulk and CeO_2-catalyzed $NaAlH_4$, respectively, and 5.5 wt.% hydrogen was released rapidly within 100 min at a temperature as low as 180 ^{o}C. Additionally, an apparent activation energy of 76.32 kJ·mol^{-1} was observed for the nanoconfined $NaAlH_4$ inside the CeO_2 HNTs, which is significantly lower than for the bulk and catalyst-doped $NaAlH_4$. This provides direct evidence for the significantly enhanced dehydrogenation kinetics due to the nanoconfinement of $NaAlH_4$ inside CeO_2 HNTs. Moreover, the novel strategy of using a scalable electrospinning technique to synthesize catalytic scaffolds that was explored in this work provides new avenues for enhancing the hydrogen storage performance of $NaAlH_4$.

Acknowledgements

This work was partially supported by the National Science Fund for Distinguished Young Scholars (51625102), the National Natural Science Foundation of China (51471053), the Science and Technology Commission of Shanghai Municipality (17XD1400700) and a Discovery Early Career Researcher Award (DE170100362). The authors also would like to thank Dr. Tania Silver for critical reading of the manuscript.

Notes and references

1 L. Schlapbach and A. Zuttel, *Nature*, 2001, **414**, 353.
2 N. S.Lewis and D. G. Nocera, *Proc. Natl. Acad. Sci. U.S.A.*, 2006, **103**, 15729.
3 P. E. de Jongh and P. Adelhelm, *ChemSusChem*, 2010, **3**, 1332.
4 G. L. Xia, D. Li, X. Chen, Y. Tan, Z. Tang, Z. Guo, H. Liu, Z. Liu, and X. Yu, *Adv. Mater.*, 2013, **25**, 6238.

5 J. Huang, L. Ouyang, Q. Gu, X. Yu, and M. Zhu, *Chem. Eur. J.*, 2015, **21**, 14931.
6 J. Yang, S. Hirano, *Adv. Mater.*, 2009, **21**, 3023.
7 U. Eberle, M. Felderhoff, F. Schüth, *Angew. Chem. Int. Ed.*, 2009, **48**, 6608.
8 B. Bogdanović and M. Schwickardi, *J. Alloys Compd*., 1997, **1**, 253.
9 B. Bogdanović, M. Felderhoff, A. Pommerin, F. Schüth and N. Spielkamp, *Adv. Mater.*, 2006, **18**, 1198.
10 G. L. Xia, Y. Tan, X. Chen, D. Sun, Z. Guo, H. K. Liu, L. Ouyang, M. Zhu, and X. Yu, *Adv. Mater.*, 2015, **27**, 5981.
11 X. Fan, X. Xiao, L. Chen, S. Li, H. Ge and Q. Wang, *J. Phys. Chem. C*, 2011, **115**, 2537.
12 X. Fan, X. Xiao, L. Chen, L. Zhang and J. Shao, *J. Mater. Chem. A*, 2013, **1**, 9752.
13 X. Zhang, Y. Liu, K. Wang, Y. Li, M. Gao and H. Pan, *ChemSusChem*, 2015, **8**, 4180.
14 C. P. Baldé, B. P. C. Hereijgers, J. H. Bitter and K. P. de Jong, *Angew. Chem. Int. Ed.*, 2006, **45**, 3501.
15 S. Zheng, F. Fang, G. Zhou, M. Zhu and D. Sun, *Chem. Mater*., 2008**, 20**, 3954.
16 P. A. Berseth, A. G. Harter, R. Zidan, A. Blomqvist and C. M. Araújo, *Nano Letters.*, 2009, **9**, 1502.
17 C. P. Baldé, O. Leynaud, P. Barnes, E. Peláez-Jiménez, K. P. de Jonga and J. H. Bitter, *Chem. Commun.*, 2011, **47**, 2143.
18 P. Adelhelm, J. Gao, M. H. W. Verkuijlen, C. Rongeat, M. Herrich and P. Jan M. van Bentum, *Chem. Mater.*, 2010, **22**, 2233.
19 J. Gao, P. Adelhelm, M. H. W. Verkuijlen, C. Rongeat, M. Herrich and P. Jan M. van Bentum, *J. Phys. Chem. C*, 2010**, 114**, 4675.
20 Y. Li, F. Fang, H. Fu, J. Qiu, Y. Song, Y. Li, D. Sun and M. Zhu, *J. Mater. Chem. A*., 2013, **1**, 5238.
21 S. Chumphongphan, U. Filsø, M. Paskevicius, D. A. Sheppard, T. R. Jensen and C. E. Buckley, *Int. J. Hydrogen Energy*, 2014, **39**, 11103.
22 R. Xiong, G. Sang, X. Yan, G. Zhang and X. Ye, *J. Mater. Chem.*, 2012, **22**, 17183.
23 Y. Li, G. Zhou, F. Fang, X. Yua, Q. Zhang, L. Ouyang, M. Zhu and D. Sun, *Acta Materialia*, 2011, **59**, 1829.
24 T. K. Nielsen, P. Javadian, M. Polanski, F. Besenbacher and T. R. Jensen, *Nanoscale*, 2013, **10**, 1039.
25 M. Paskevicius, U. Filsø, F. Karimi, J. Puszkiel, P. K. Pranzas, C. Pistidda and A. Hoell, *Int. J. Hydrogen Energy*, 2016, **41**, 4159.
26 X. Fan, X. Xiao, J. Shao, L. Zhang, S. Li, H. Ge, Q. Wang and L. Chen, *Nano Energy*, 2013, **2**, 995.
27 V. Stavila, R. K. Bhakta, T. M. Alam, E. H. Majzoub and M. D. Allendorf, *ACS Nano*, 2012, **6**, 9807.
28 R. K. Bhakta, J. L. Herberg, B. Jacobs, A. Highley, R. Behrens and M. D. Allendorf, *J. Am. Chem. Soc.*, 2009, **131**, 13198.
29 T. K. Nielsen, M. Polanski, D. Zasada, P. Javadian, F. Besenbacher and J. Bystrzycki, *ACS Nano*, 2011, **5**, 4056.
30 E.H. Majzoub, F. Zhou and V. Ozoliņš, *J. Phys. Chem. C*, 2011, **115**, 2636.
31 W. Lohstroh, A. Roth, H. Hahn and M. Fichtner, *ChemPhysChem*, 2010, **11**, 789.
32 Y. Cheng, B. Zou, C. Wang, Y. Liu, X. Fan, L. Zhu, Y. Wang, H. Ma and X. Cao, *CrystEngComm*, 2011, **13**, 2863.
33 L. Xu, H. Song, B. Dong, Y. Wang, J. Chen, and X. Bai, *Inorg. Chem.*, 2010, **49**, 10590.
34 S. M. Hwang, S. Y. Kim, J-G. Kim, K. J. Kim, J-W. Lee, M-S. Park, Y-J. Kim, M. Shahabuddin, Y. Yamauchif and J. H. Kim, *Nanoscale*, 2015, **7**, 8351.
35 T. K. Nielsen, P. Javadian, M. Polanski, F. Besenbacher, J. Bystrzycki and T. R. Jensen, *J. Phys. Chem. C*, 2012, **116**, 21046.
36 J. Hu, S. Ren, R. Witter and M. Fichtner, *Adv. Energy Mater*., 2012, **2**, 560.
37 A. Leon, J. Rothe, K. Chlopek, O.Zabara and M. Fichtner, *Phys. Chem. Chem. Phys.*, 2009, **11**, 8829.
38 T. Mueller, G. Ceder, *ACS Nano* 2010, **4**, 5647.
39 D. Pukazhselvan, M. S. L. Hudson , A. S. K. Sinha, O. N. Srivastava, *Energy*, 2010, **35**, 5037.
40 X. Fan, X. Xiao, L. Chen, S. Li and Q. Wang, *J. Alloys Compd.*, 2011, **509**, S750.